High-K tungsten-mullite composite for electronic industrial application: synthesis and study of its microstructure, phase behavior and electrical properties

Kumaresh Halder · Biplab Kumar Paul ·
Debasis Roy · Alakananda Bhattacharya ·
Sukhen Das

Abstract Highly crystallized mullite synthesis with different concentration of tungsten ions has been achieved by sol–gel technique and the effect of tungsten ion doping on mullite was examined at 1,100 and 1,400 °C. Characterizations were done by DTA/TGA, XRD, FTIR, LCR and FESEM instruments at the room temperature. Mullite formation was found to depend on the concentration of the doping ion up to a certain extent. With the addition of tungsten ion, the mullite formation temperature was decreased. The result showed a decrease in mullite phase at higher concentrations of doping ion with respect to undoped mullite. Oxide phases continued to increase with increasing doping concentration, which is mainly responsible for the increment in dielectric value. Dielectric value of the doped mullite was found to decrease with the increase in frequency for all the samples and saturates at higher frequency, which is normal behavior for dielectric ceramics. A.C. conductivity increased with frequency by following Jonscher's power law. The composite showed maximum dielectric constant of 124.02 sintered at 1,400 °C for 0.05 M at 20 Hz frequency. Highly crystalline mullite whiskers of average dimension 3 μm were obtained at 0.02 tungsten concentration sintered at 1,400 °C. Due to the good dielectric response, comparatively low loss and appropriate nature of the doped mullite it can be used as ceramic capacitors, packaging material for integrated high speed devices. Also, it's electrical and thermal suitability may prove to be significant as the insulator material of the spark plug.

K. Halder · B. K. Paul · D. Roy · A. Bhattacharya · S. Das (✉)
Department of Physics, Jadavpur University, Kolkata 700 032, India
e-mail: sukhenjudas@gmail.com

1 Introduction

Mullite ($3Al_2O_3 \cdot 2SiO_2$) is a promising candidate of traditional and advanced ceramics because of its outstanding electrical, mechanical and thermal properties such as high melting point, good creep resistance, superior high temperature strength, low thermal expansion, thermal shock resistance, exceptional chemical stability under harsh chemical environments etc [1–6]. Advanced structural ceramics have a great contribution in electronics industries with its unique structural, optical and dielectric applications. Fundamental building unit in mullite is the chain of edge-sharing AlO_6-octahedra oriented parallel to the crystallographic c-axis. These chains of octahedra are separated by $(Si, Al)O_4$ tetrahedra in an alternating sequence, forming double chains parallel to the c-axis [7–9]. The topological arrangement of these chains is a common feature of a whole group of compounds with various chemical compositions. Conventionally, mullite formation starts above 1,200 °C completing at around 1,600 °C by solid state reaction between aluminium oxide (Al_2O_3) and silicon dioxide (SiO_2) particles [10–14]. Here mullite precursors are mixed at atomic level which is best achieved via sol–gel route by using a salt of aluminium and tetraethyl orthosilicate (TEOS). Sol–gel route is the most preferred way till date because of the chemical homogeneity of the precursors and high purity of the end product [15–17].

The 3:2 mullite has a highly stable open structure ($T_{Melt} = 1,828 \pm 10$ °C) and it can accommodate a variety of transition metal ions into its structure as a solid solution [18, 19]. Transition metal generally induces their effects by interacting with the silica layer and destabilizing the aluminium–silicate matrix [20–23]. Such solid solutions can result in desirable improvements in physical properties. Many reports have been published in the recent times

regarding synthesis of mullite composites, in presence of various metal ions with the aim, to improve the properties of modified mullite composites. From these studies it has been concluded that the mullite structure can incorporate differing amounts of ions, where the limit of dopant ion incorporation depends on synthesis conditions, ionic radii and the oxidation states of transition metal ions [24].

A spark plug contains an insulator as a basic building block of its body parts, where a ceramic material (e.g. mullite) is used as an insulator. The insulator is used to isolate the high voltage at the electrodes, ensuring the spark happens at the tip of the center electrode and not anywhere else on the plug. The insulator is subjected to harsh conditions so a considerably high dielectric strength and adequate thermal conductivity is required [25, 26]. Generally mullite is ceramic material with low dielectric constant (~ 6). Through systematic investigation it can be seen that, dielectric value became much higher for tungsten doped mullite, which is suitable to be the ceramic material of the spark plug.

2 Experimental procedure

2.1 Materials

Chemicals used in the preparation of mullite precursor gels are: Aluminium nitrate nonahydrate ($Al(NO_3)_3 \cdot 9H_2O$) extra pure (MERCK, India), Aluminium isopropoxide ($Al(-O-i-Pr)_3$) puriss (Spectrochem Pvt. Ltd., India.), Tetra ethyl orthosilicate ($Si(OC_2H_5)_4$) (MERCK, Germany) and Phosphotungstic acid ($H_3[P(W_3O_{10})_4] \times H_2O$) (MERCK, Germany).

2.2 Methods

Aluminum isopropoxide and aluminum nitrate nonahydrate (ANN) were used as the alumina sources, whereas tetra ethyl orthosilicate (TEOS) was used as a source of silica. By using aluminium nitrate nonahydrate a 0.5 M aqueous solution was prepared. Mullite precursor gel powder was synthesized by dissolving stoichiometric amounts of aluminium isopropoxide and TEOS in the aqueous solution of aluminium nitrate nonahydrate. The molar ratio of $Al(-O-i-Pr)_3/Al(NO_3)_3 \cdot 9H_2O$ was kept at 7:2 in order to form spinnable sols and the mole ratio of Al/Si was 3:1. Moreover, pH of the solution was also maintained at 5. On vigorous stirring for 2 h and overnight temperature treatment at 60 °C, the solutions forms gel which was further dried and mortared to form a free flow powder.

By adding aqueous solution of five different concentrations of the tungsten salts—0.002, 0.005, 0.01, 0.02, and 0.05 M to the undoped mullite solution and stirring it for

120 min, metal ion doped gels were prepared by sol–gel method. Then the above mentioned procedure is repeated to obtain free flow powder of doped mullite. The samples were then pelletized and sintered at 1,100 and 1,400 °C for 3 h in a muffle furnace under air atmosphere (heating rate 10 °C/min.). This whole process is summarized as a flowchart shown in Fig. 1.

2.3 Investigating instruments

The crystalline phases developed in the samples sintered at 1,100 and 1,400 °C were analyzed by X-ray powder diffractometer (model-D8, Bruker AXS, Wisconsin, USA) using Cu Kα radiation—1.5418 Å and operating at 40 kV with a scan speed of 1 s/step.

The characteristic stretching and bending modes of vibration of chemical bonds of samples were effectively evaluated by FTIR spectroscopy (FTIR-8400S, Shimadzu). The samples were pelletized after mixing 1 % sample with spectroscopy grade KBr and then analyzed by FTIR using pure KBr pellet as background from 1,600 to 400 cm^{-1}.

Thermal behavior of the gel samples were investigated by a DTA-TGA [DTG-60H, Shimadzu (Asia Pacific) pvt. Ltd., Singapore] analyzer operated at the heating rate of 10 °C/min under N_2 flow.

Electrical properties such as dielectric constant (ε_r), dissipation factor (tanδ), A.C. conductivity ($\sigma_{a.c.}$), resistivity (ρ) of the samples were measured in the frequency range 20 Hz–2.0 MHz using LCR meter (HP Model 4,274
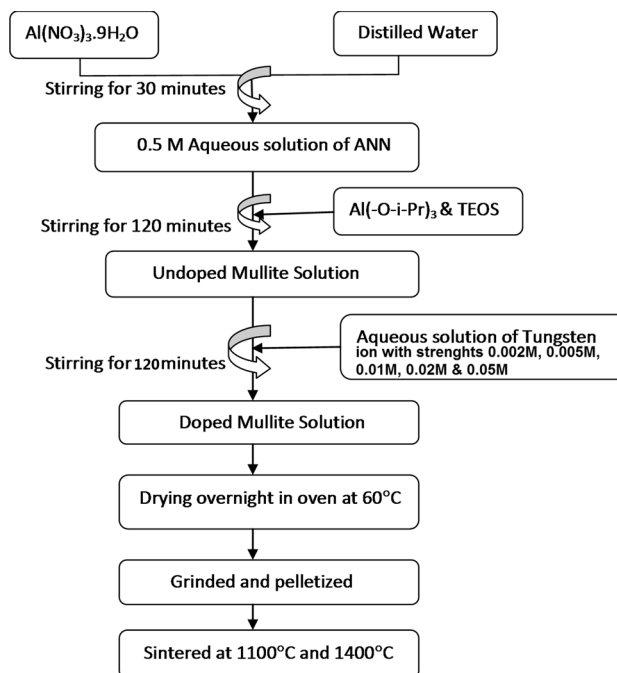

Fig. 1 Flowchart depicting formation of tungsten doped mullite

A, Hewlett-Packard, USA). For the measurement of electrical properties sample pellets of uniform thickness were prepared, and silver paste was coated on two extreme surfaces of the pallet to make those surfaces conducting.

The morphology of the sintered gels were studied by field emission scanning electron microscope (FESEM) (JSM 6700F, JEOL Ltd., Tokyo, Japan). Samples were etched with 25 % HF solution and about 2 mg of each sample was dispersed in ethanol and a single drop was placed on copper grid for sample preparation.

3 Results and discussion

3.1 DTA/TGA analysis

The DTA/TGA curves shown in Fig. 2a, b provides comparable differences between thermal behaviors of undoped mullite gel and the gel having higher concentration of tungsten ion as dopant. From the DTA pattern it can be seen that, in both cases there are two endothermic peaks below 400 °C, due to the evolution of volatile components e.g. water, alcohol from the surface and structure. Here we can notice that, for undoped mullite gel there is a sharp exothermic peak at 961.89 °C. The occurrence and intensity of this exothermic peak are closely related to the intimacy and homogeneity of the Al–Si components in the gels. Upon addition of tungsten ion, an exothermic peak is obtained at 782.09 °C which is shifted towards lower temperature by 179.80 °C compared to undoped one. This transformation was achieved due to the complex forming ability of the transition metal ions in the alumino-silicate matrix [18, 19]. Hence we can conclude that, for the gel with higher concentration of tungsten, temperature of

mullite formation has decreases due to the melting of tungsten, which decreases the viscosity and helps in mullite formation at a comparatively low temperature. On the other hand, TGA curve shows that there occurs considerable weight loss in between 30 and 400 °C due to evaporation of water contents, alcohol etc. and no additional significant weight loss is seen up to 1,400 °C.

3.2 X-ray diffraction analysis

Here crystal phase developments are observed at two different temperatures 1,100 and 1,400 °C.

In the X-ray diffractograms it has been observed that the undoped sample shows considerable mullite phase at 1,100 and 1,400 °C, similarly the doped samples exhibit prominent mullite phase (JCPDS # 15-0776) which varies with the variation of the concentrations. Mullite phase increases with increasing concentration of metal ions up to 0.01 M at 1,100 and 1,400 °C, then yield of mullite phase decreases (Fig. 3a, b).

This suggests that at low concentration tungsten ion can effectively induce accelerated transformation of the gels into mullite, but on reaching a critical concentration, the gel cannot transform into mullite. In fact at higher concentrations, tungsten doped gels transforms to crystalline aluminium oxide (JCPDS # 0.43-1484), tungsten oxide (JCPDS # 44-0396), silicon tungsten oxide (JCPDS # 0.25-1331) and the aluminum tungsten oxide (JCPDS # 29-0096) phases (Fig. 3b). At higher doping concentrations, the initial gel formation became inhomogeneous due to the excess metal ion [20–22].

The sharp peaks at 1,400 °C indicates complete mullitization expected at such high temperature, whereas, in case of tungsten doped mullite sintered at 1,100 °C, there
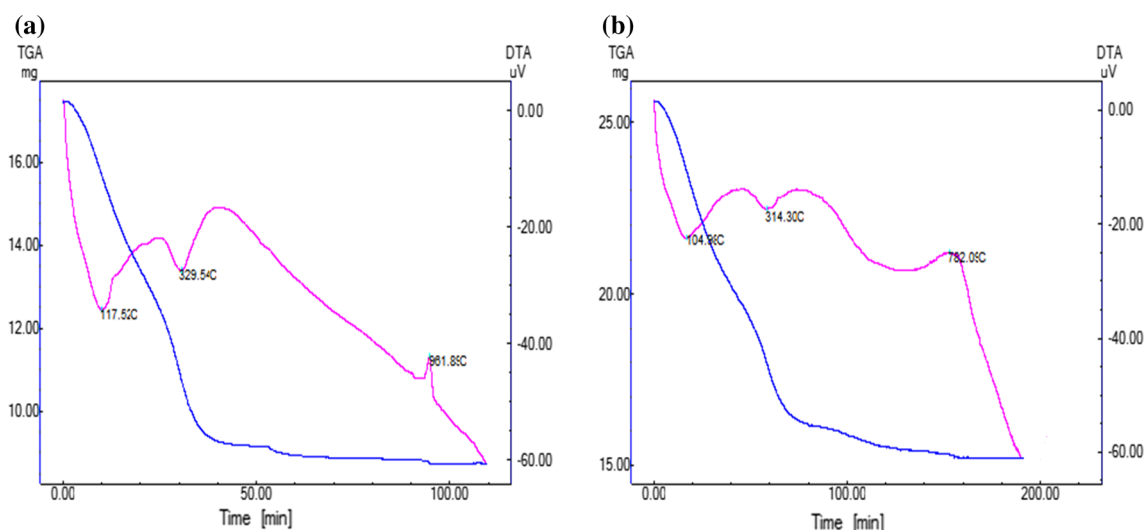

Fig. 2 **a**, **b** DTA/TGA pattern of undoped (G$_0$) and doped mullite gel with higher concentration (0.05 M) of tungsten ion
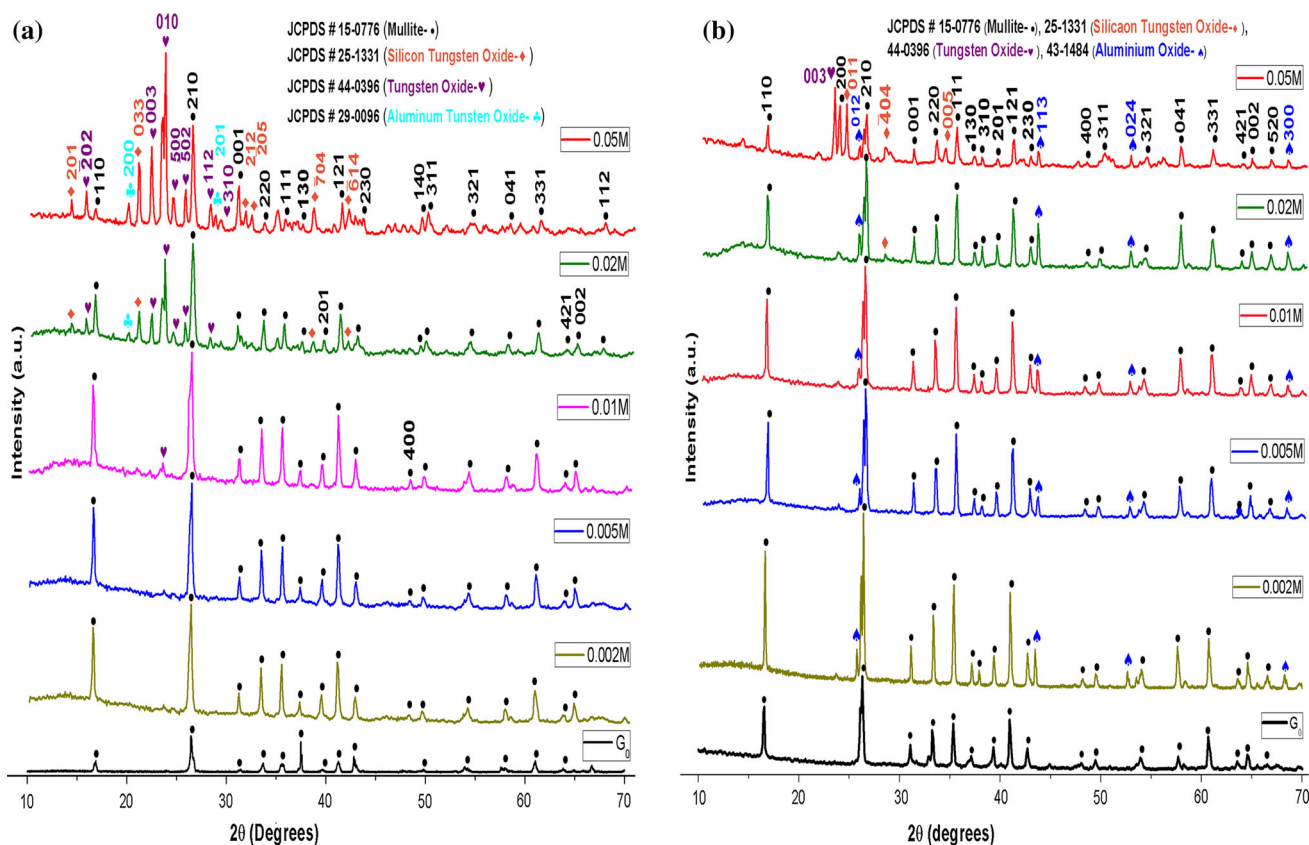
Fig. 3 a, b XRD plot of tungsten doped mullite of different concentrations sintered at 1,100 and 1,400 °C

still remains amorphous phases, which accounts in formation of peaks relatively blunt compared to the mullite sintered at 1,400 °C.

3.3 FTIR analysis

The infrared spectra of tungsten doped mullite of different strengths along with pure mullite sintered at 1,100 and 1,400 °C were recorded in the range of 1,350–450 cm^{-1}. In the spectrum of pure mullite gel (G$_0$), calcinated at 1,100 °C, it gives peaks around wave number 1,136, 866, 740, 579, 517 cm^{-1}. It is reported that, development of a shoulder near about 1,130 cm^{-1} is assigned to the asymmetric Si–O stretching vibration of SiO$_4$ tetrahedra, Al–O tetrahedral condition gives Al–O stretching modes in the region 750–850 cm^{-1}, and an Al–O octahedral condition gives Al–O stretching modes in the region 500–750 cm^{-1}, which are the characteristic bands of mullite [22–24, 27]. Similarly doped samples of strengths 0.002, 0.005, 0.01, 0.02, 0.05 M sintered at above mentioned temperatures, shows all the characteristic bands of mullite (Fig. 4a).

In case of pure mullite (G$_0$) gel calcinated at 1,400 °C peaks are obtained around 1,176, 1,133, 911, 831, 750 and 570 cm^{-1}. Here the shoulders at 1,176 and 1,133 cm^{-1} are

assigned respectively, to the asymmetric stretching vibrations of Si–O–Si and Si–O–Al networks [28]. Shifting of asymmetric stretching frequencies to the higher wave number indicates the better formation of mullite at 1,400 °C; this is further confirmed by the FESEM images. Other peaks at 831 (alumina tetrahedra), 750 (alumina tetrahedra), 570 (alumina octahedra) further confirms the formation of mullite. Doped samples of five above mentioned strengths sintered at 1,400 °C, exhibits all the characteristics peak of mullite along with a peak 624 cm^{-1} which may be due to the W–O bond in tungsten oxide phases as shown in Fig. 4b.

3.4 Electrical properties analysis

3.4.1 Dielectric analysis

Dielectric constant of each sample was calculated by using the formula

$$\varepsilon_r = (C \times d)/A\varepsilon_0$$

where, C, d, A, ε_r and ε_0 are the capacitance of material, thickness of the pellet, area of cross-section, dielectric constant and permittivity of free space respectively [29].
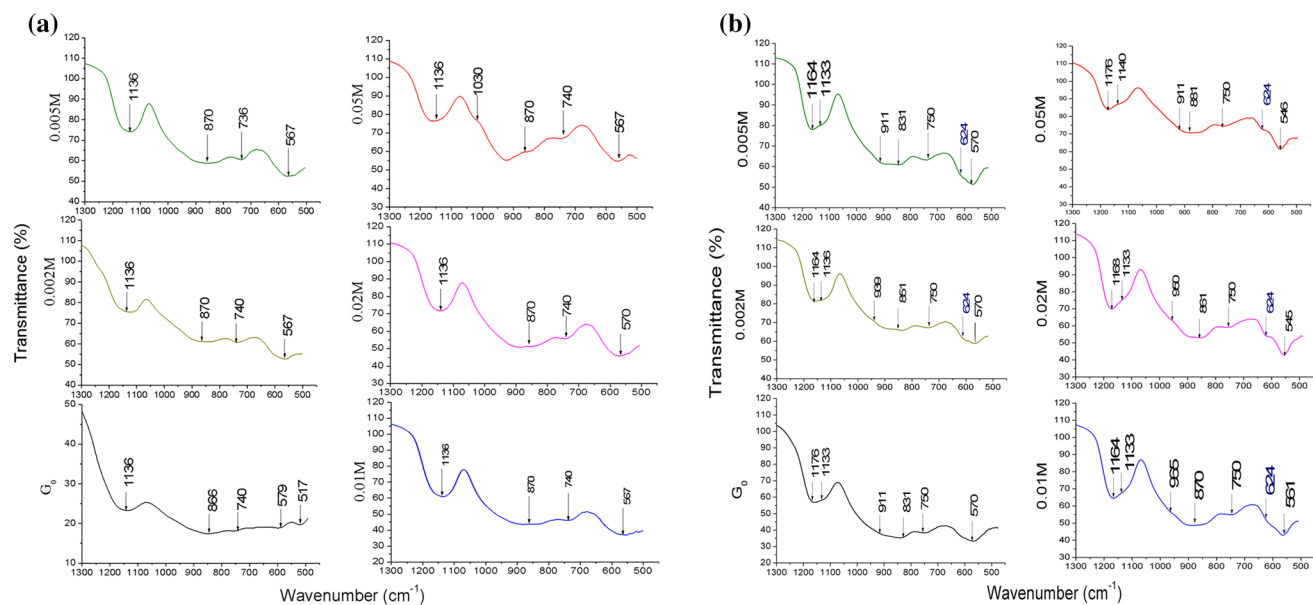
Fig. 4 **a**, **b** FTIR bands of tungsten doped mullite precursor gels sintered at 1,100 and 1,400 °C

The variation of dielectric constant of tungsten doped mullite with frequency fired at 1,100 and 1,400 °C are shown in Fig. 5a, b. From the plot it is observed that in all the cases dielectric constant decreases with increase in frequency. It happens as the electrode blocking layer is the dominating mechanism at lower frequency region; thus the dielectric behavior is affected by electrode polarization. At higher frequency the dipole cannot rotate sufficient rapidly results a lag in oscillation behind the field. As the frequency is increased further, the dipole will be completely unable to follow the field, so it approaches a constant value at higher frequencies [30]. Presence of tungsten increases

the value of dielectric constant and it increases smoothly with an increase in concentration of tungsten as it was attributed to interfacial polarization [31]. At 20 Hz, 0.05 M tungsten doped mullite composite gave k value (dielectric constant) of 81.23 and 124.02 fired at 1,100 and 1,400 °C respectively.

3.4.2 Dissipation factor analysis

The dielectric loss (tanδ) of all samples was measured in the frequency range 20 Hz–2.0 MHz in the room temperature and is graphically shown in Fig. 6a, b. At lower

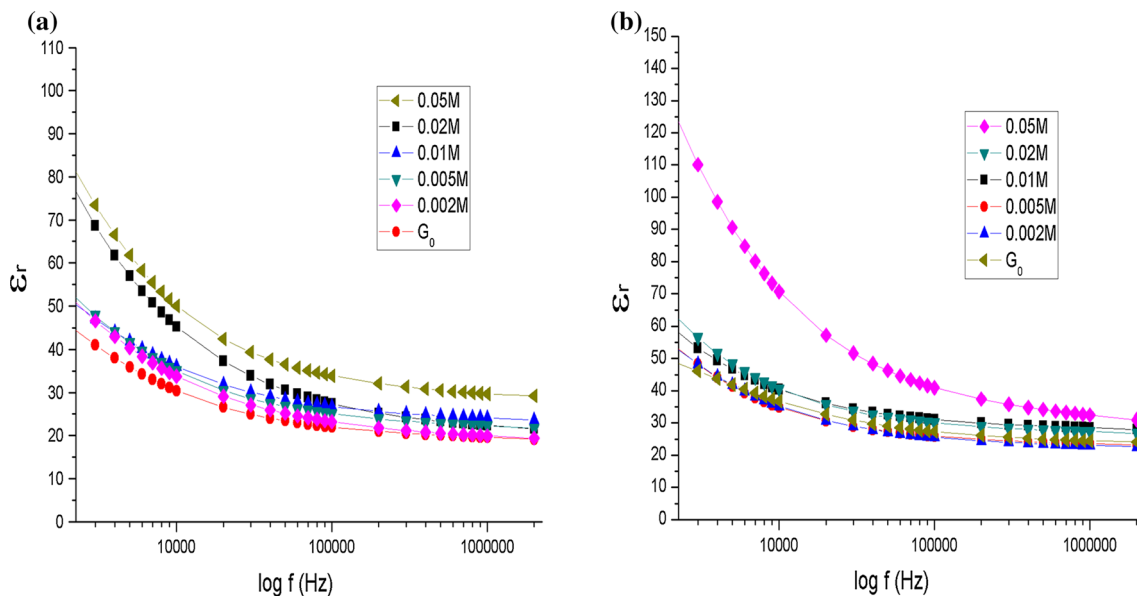**Fig. 5** **a**, **b** Variation of dielectric constant (ε_r) with log f(Hz) of mullite gels sintered at 1,100 and 1,400 °C

frequencies, tanδ is large for all samples and decreases with increasing frequency reaching a constant value. The reason behind is that in low signal frequency range electrical dipoles follows the variation of electric field and it reaches constant value at 2.0 MHz [32]. Dielectric loss increases linearly with increasing dopant ion content in investigated frequency range. The tangent loss for composites is large at 1,100 °C; as after sintering at 1,100 °C for 3 h, the ceramic composites still remains amorphous, whereas, tangent loss decreases to a pretty small value of all strengths at 1,400 °C, as at this temperature the crystallinity of mullite increases.

3.4.3 A.C. Conductivity analysis

Electrical conductivity (σ_{total} (ω)) consists of two parts: A.C. conductivity ($\sigma_{a.c.}(\omega)$) and D.C. conductivity ($\sigma_{d.c.}$). During a.c. conductivity the frequency of the electric field varies whereas in case of d.c. conductivity it remains constant. $\sigma_{d.c.}$ depends strongly on temperature and dominate on low frequency and high temperature. $\sigma_{a.c.}$ (ω) has a dependence on temperature and dominates at higher frequency and low temperature. The relation for frequency dependent ac conductivity is

$$\sigma_{a.c.}(\omega) = A\omega^s,$$

where, A is constant, S is a function of temperature, value of which lies in between 0 and 1 [33–35].

The plot of log $\sigma_{a.c.}(\omega)$ versus log f shows a linear increment of a.c. conductivity with frequency for all doping concentrations as shown in Fig. 7a, b. Increase of frequency increased a.c. conductivity by increasing hopping of conducting electrons present in tungsten mullite composite. At higher frequency the hopping frequency could not match the applied field frequency [36]. Presence of tungsten ion in the mullite structure increases the mobility of ions, so a.c. conductivity increases with the increasing concentration of tungsten. The increase of conductivity at lower frequency range is due to interfacial polarization; as the conductivity is pure d.c. in this region [37]. At higher frequency range, rapid increase of conductivity with increasing frequency is referred to electronic polarization effect.

3.4.4 Resistivity analysis

Although the thermal conductivity is the most important property for heat sink and electrical contact applications, this property is not easy to measure due to large experimental errors. Since resistivity (ρ) is easy to measure and can be translated into thermal conductivity when needed through the Wiedmann–Franz equation, it was selected in this study to compare the thermal properties of the tungsten doped mullite. For metals, thermal conductivity is considerably high and those metals which are good electrical conductors are also good thermal conductors, as we know that, at a given temperature thermal conductivity of a metal is proportional to its electrical conductivity [38]. Figure 8a, b shows that the resistivity decreases with increasing density of the dopant ion. Generally mullite is a bad
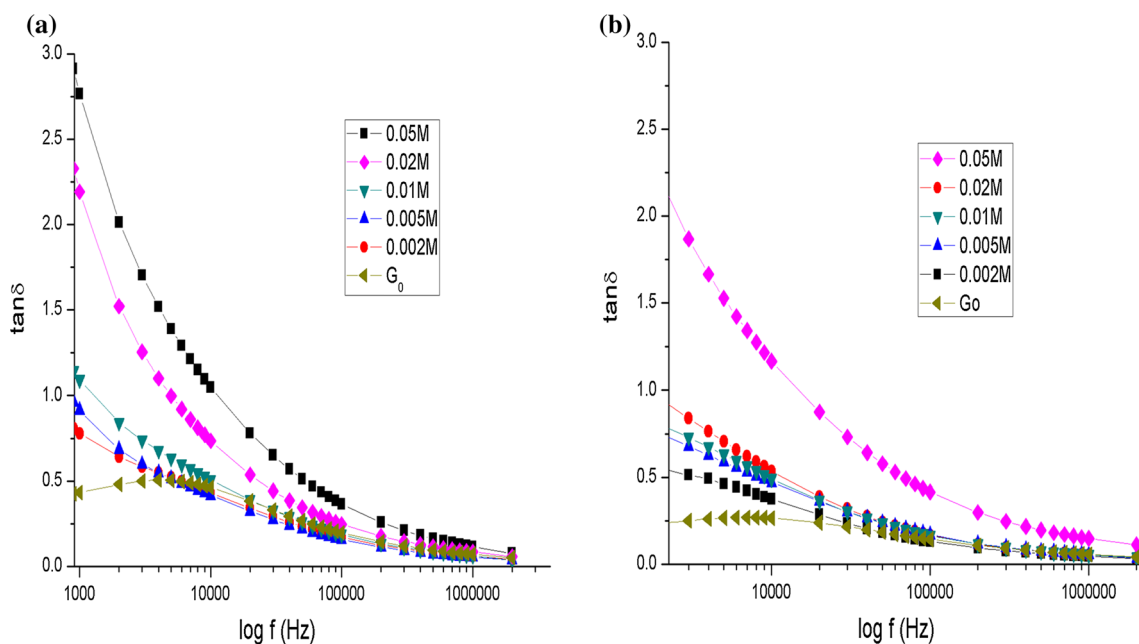

Fig. 6 a, b Variation of dielectric loss (tanδ) with log f(Hz) of mullite gels sintered at 1,100 and 1,400 °C
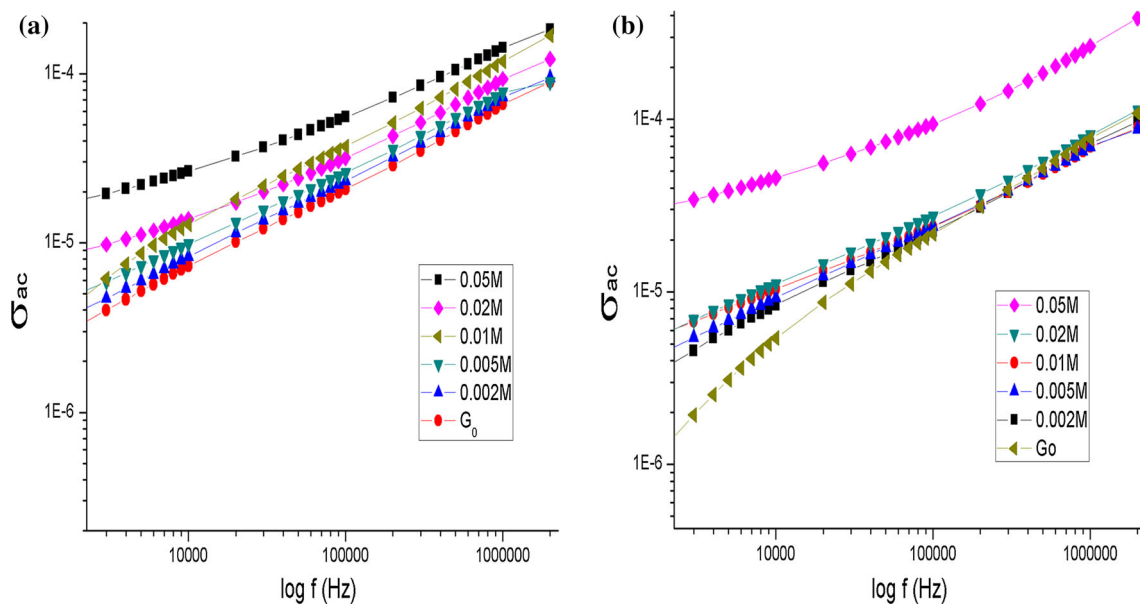
Fig. 7 **a**, **b** Variation of log of AC conductivity (log $\sigma_{a.c.}(\omega)$) with log f(Hz) of mullite gels sintered at 1,100 and 1,400 °C

conductor, so it is found to be a highly resistive material, but when we incorporate some conducting metal like tungsten in it, the resistivity began to decrease as the conductivity grows in it, and as the electrical conductivity increases, thermal conductivity also increases by the Wiedmann–Franz equation:

$$\frac{\gamma}{\sigma} = LT,$$

where, γ is thermal conductivity, L is Lorenz number, which is constant for all metals (2×10^{-8} W Ω K^{-2}), T is

absolute temperature [38]. Thus resistivity decreases as electrical conductivity is inversely proportional to electrical resistivity.

The factors, which are responsible for lowering of resistivity of mullite are, the 3-D orbital electrons, the oxidation states and the concentration of the transition metal ions as well as the sites of mullite lattice occupied by the ions [39, 40].

From the plot it is observed that, at 2 MHz frequency the resistivity of pure mullite sample are 419.81 and 291.56 Ω cm, where, for doped samples of highest strength
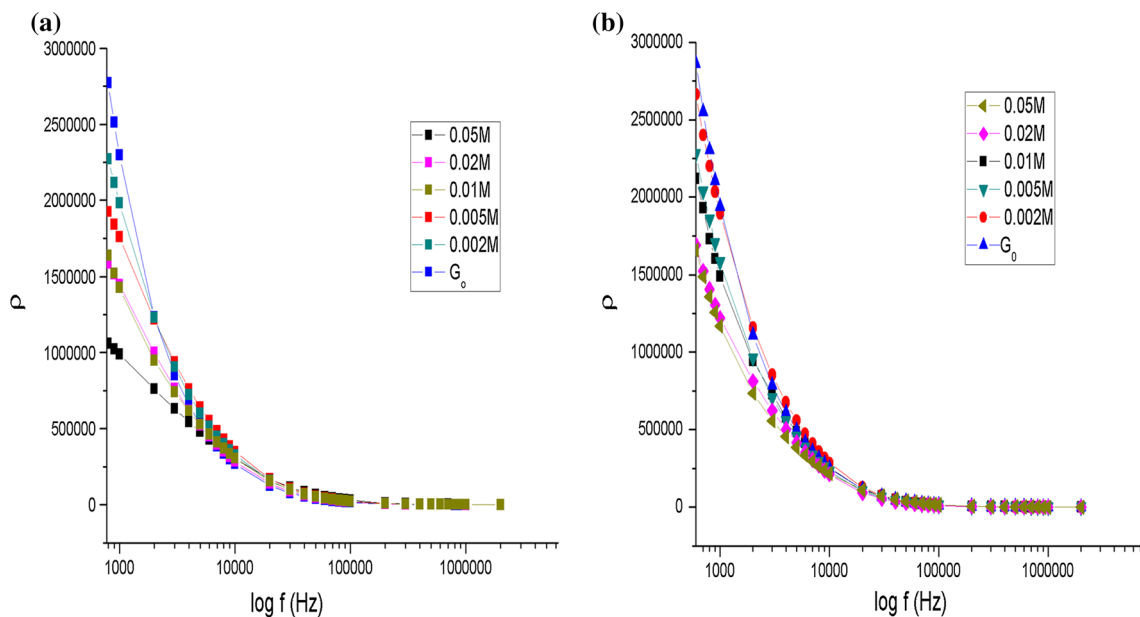

Fig. 8 **a**, **b** Variation of resistivity (ρ) with log f(Hz) of mullite gels sintered at 1,100 and 1,400 °C

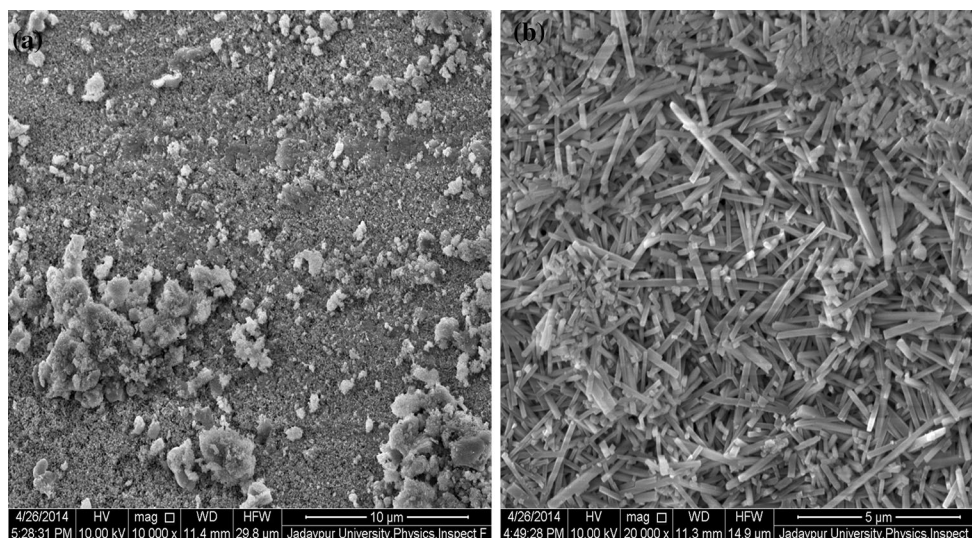**Fig. 9** **a**, **b** FESEM analysis of tungsten doped mullite of highest concentration (0.05 M) sintered at 1,100 and 1,400 °C

(0.05 M) it became 209.49 and 149.06 Ω cm, sintered at 1,100 and 1,400 °C respectively. Thus, due to incorporation of tungsten in mullite, its electrical resistivity has been reduced to almost half of its primary value; accordingly the thermal conductivity of the composite sintered at above mentioned temperatures will reflect considerably commendable values.

3.5 FESEM analysis

The microstructure of the mullite particle of highest (0.05 M) concentration of the doped transition metals was investigated by FESEM for 1,100 and 1,400 °C. 0.05 M tungsten doped mullite fired at 1,100 °C (Fig. 9a) shows complete different behavior from the doped mullite fired at 1,400 °C (Fig. 9b). The micrograph in Fig. 9a shows almost spherical morphology of mullite with amorphous aggregates and open spaces, whereas Fig. 9b shows uniform microstructure, which is composed of large anisotropic grains or whiskers. Distinct mullite particles of average size of 3 μm were seen embedded in the matrix of Fig. 9b.

It can be concluded from the observations that, doped sample fired at 1,100 °C was insufficient to produce mullite whiskers, as there were few amorphous phases, which is evident from the XRD analysis.

4 Conclusion

Tungsten doped mullite composites have been synthesized by sol–gel technique and their phase evolution and electrical properties have been investigated. Concentration of the ions and temperature are the two primary factors found to affect the formation of mullite. With increase in concentration of doping ion up to a certain value, extent of mullite formation has been found to increase, and then it began to decrease, as it gives rise to other oxides. The observations of the present research work indicate that the electrical properties can be enhanced by doping tungsten ion. The dielectric constant of doped mullite has been found to be high and it decrease with increase in frequency. The highest dielectric constant is about 124.02 at 20 Hz for tungsten-mullite composite sintered at 1,400 °C for 0.05 M. A.C. conductivity increases with frequency and depending on the concentration of mobile ions present in the composites. Also the resistivity of the doped ceramics began to decrease with the increase in frequency and the incorporation of the transition metal ions, the dopants, alone could reduce the electrical resistivity of mullite.

From all the above mentioned analysis, it can be concluded that, the doped mullite may be used for the fabrication of ceramic capacitors in the pico range. Also, this composite can withstand very high temperatures of about 1,400 °C. The dielectric strength and its resistivity also suit the doped ceramic as the insulating material of the spark plug.

References

1. K.S. Mazdiyasni, L.M. Brown, Synthesis and mechanical properties of stoichiometric aluminum silicate (mullite). J. Am. Ceram. Soc. **55**, 548–552 (1972)

2. B.L. Metcalfe, J.H. Sant, Synthesis, microstructure, and physical properties of high purity mullite. Trans. J. Br. Ceram. Soc. **74**, 193–201 (1975)

3. S. Kanzaki, H. Tabata, T. Kumazawa, S. Ohta, Sintering and mechanical properties of stoichiometric mullite. J. Am. Ceram. Soc. **68**, C6–C7 (1985)

4. V.V. Vol'khin, I.L. Kazakova, P. Pongratz, E. Halwax, Mullite formation from highly homogeneous mixtures of Al_2O_3 and SiO_2. Inorg. Mater. **36**(4), 375–379 (2000)

5. H. Schneider, J. Schreuer, B. Hildmann, Structure and properties of mullite: a review. J. Eur. Ceram. Soc. **28**(4), 329–344 (2008)

6. S. Rahman, S. Freimann, The Real Structure of Mullite, in *Mullite*, ed. by H. Schneider, S. Komarneni (Wiley-VCH, Weinheim, 2005), pp. 46–70

7. H. Schneider, S. Komarneni, *Mullite*, 2nd edn. (Wiley-VCH, Weinheim, 2006)

8. R.J. Angel, C.T. Prewitt, Crystal-structure of mullite: a re-examination of the average structure. Am. Mineral. **71**, 1476–1482 (1986)

9. S. Durovic, P. Fejdi, Synthesis and crystal structure of germanium mullite and crystallochemical parameters of D-mullites. Silikaty **2**, 97–112 (1976)

10. H. Saalfeld, V. Guse, Structure refinement of 3-2-mullite ($3Al_2O_3 \cdot 2SiO_2$). Neues Jahrbuch Fur Mineralogie-Monatshefte **4**, 145–152 (1981)

11. F. Sahnoune, M. Chegaar, N. Saheb, P. Goeuriot, F. Valdivieso, Algeria kaolinite used for mullite formation. Appl. Clay Sci. **38**, 304–310 (2008)

12. H.F. Chen, M.C. Wang, M.H. Hon, Phase transformation and growth of mullite in kaolin ceramics. J. Eur. Ceram. Soc. **24**, 2389–2397 (2004)

13. V. Viswabaskarana, F.D. Gnanama, M. Balasubramanian, Mullite from clay-reactive alumina for insulating substrate application. Appl. Clay Sci. **25**, 29–35 (2004)

14. V. Viswabaskarana, F.D. Gnanama, M. Balasubramanian, Mullitisation behavior of calcined clay–alumina mixtures. Ceram. Int. **29**(5), 561–571 (2003)

15. D.J. Cassidy, J.L. Woolfrey, B.R. Bartlett, B. Ben-Nissan, The effect of precursor chemistry on the crystallization and densification of sol–gel derived mullite gels and powders. J. Solgel Sci. Technol. **10**, 19–30 (1997)

16. A.M.L. Marques Fonseca, J.M.E. Ferreira, I.M. Miranda Salvado, J.L. Baptista, Mullite based compositions prepared by sol–gel techniques. J. Solgel Sci. Technol. **8**, 403–407 (1997)

17. Y.X. Huang, A.M.R. Senos, J. Rocha, J.L. Baptista, Gel formation in mullite precursors obtained via tetra ethyl orthosilicate (TEOS) pre-hydrolysis. J. Mater. Sci. **32**, 105–110 (1997)

18. F. Mizukami, K. Maeda, M. Toba, T. Sano, S.I. Niwa, Effect of organic ligand used in sol–gel process on the formation of mullite. J. Solgel Sci. Technol. **8**, 101–106 (1997)

19. H. Schneider, Transition metal distribution, in *Mullite and Mullite Matrix Composites*, ed. by S. Somiya, R.F. Davis, J.A. Pask (The American Ceramic Society, Westerville, 1990), p. 135

20. P. Sarin, W. Yoon, R.P. Haggerty, C. Chiritescu, N.C. Bhorkar, W.M. Kriven, Effect of transition-metal-ion doping on high temperature thermal expansion of 3:2 mullite: an in situ, high temperature, synchrotron diffraction study. J. Eur. Ceram. Soc. **28**, 353–365 (2008)

21. E.E. Kiss, P.S. Putanov, Influence of transition metal ions on the textural properties of alumina and aluminosilicate. React. Kinet. Catal. Lett. **75**(1), 39–45 (2002)

22. D. Roy, B. Bagchi, S. Das, P. Nandy, Electrical and dielectric properties of sol–gel derived mullite doped with transition metals. Mater. Chem. Phys. **138**(1), 375–383 (2013)

23. A. Beran, D. Voll, H. Schneider, Dehydration and structural development mullite precursors: an FTIR spectroscopic study. J. Eur. Ceram. Soc. **21**(14), 2479–2485 (2001)

24. S. Shoval, M. Boudeulle, S. Yariv, I. Lapides, G. Panczer, Micro-raman and FT-IR spectroscopy study of thermal transformation of St. Claire dickite. Opt. Mater. **16**, 319–327 (2001)

25. S.P. Chaudhuri, S.K. Patra, A.K. Chakraborty, Electrical resistivity of transition metal ion doped mullite. J. Eur. Ceram. Soc. **19**, 2941–2950 (1999)

26. W.J. Walker, M.E. Saccoccia, Alumina ceramic for spark plug insulator, U.S. Patent No. 20110077141 A1 (2011)

27. Ph. Colomban, Structure of oxide gels and glasses by infrared and Raman scattering: I. aluminus. J. Mater. Sci. **24**, 3002–3010 (1989)

28. M. Daniele, V. Mario, B. Guido, Mullite type structures in the system Al_2O_3–Me_2O (Me = Na, K) and Al_2O_3–B_2O_3. J. Am. Ceram. Soc. **75**, 1929–1934 (1992)

29. P. Padmaja, G.M. Anilkumar, P. Mukundan, G. Aruldhas, K.G.K. Warrier, Characterisation of stoichiometric sol–gel by Fourier transform infrared spectroscopy. Int. J. Inorg. Mat. **3**, 693–698 (2001)

30. D.R. Patil, S.A. Lokare, R.S. Devan, S.S. Chougule, C.M. Kanamadi, Y.D. Kolekar, B.K. Chougule, Studies on electrical and dielectric properties of $Ba_{1-x}Sr_xTiO_3$. Mater. Chem. Phys. **104**, 254–257 (2007)

31. R.A. Abbas, Studing some dielectric properties and effective parameters of composite materials containing of novolak resin. J. Eng. Technol. **8**(25), 277–288 (2007)

32. A. See, J. Hassan, M. Hashim, W.M.D.W. Yusoff, Dielectric variations of barium titanate additions on mullite–kaolinite sample. Solid State Sci. Technol. **16**, 197–204 (2008)

33. G.M. Tsangargi, G.C. Psarras, A.J. Kontopoulos, Dielectric permittivity and loss of an aluminum-filled epoxy resin. J. Compos. Mat. **41**, 403–417 (2007)

34. G.C. Psarras, E. Manolakaki, G.M. Tsangaris, Dielectric dispersion and ac conductivity in—iron particles loaded—polymer composites. Compos. Part A Appl. Sci. Manuf. **34**(12), 1187–1198 (2003)

35. M. Al-Haj Abdallah, Y. Alramadin, M. Ahmad, A. Zihlif, S. Jawad, A. Alnajjar, Electrical characterization of metal fiber-polyester composite. Int. J. Polym. Mat. **37**, 33–42 (1997)

36. S. Sindhu, M.R. Anantharaman, B.P. Thampi, K.A. Malini, P. Kurian, Evaluation of a.c. conductivity of rubber ferrite composites from dielectric measurements. Bull. Mater. Sci. **25**(7), 599–607 (2002)

37. L.H. VanVlack, *Elements of Material Science and Engineering*, 6th edn. (Addison-Wesley Co, New York, 1989), p. 399

38. G.C. Psarras, E. Manolakaki, G.M. Tsangaris, Electrical relaxations in polymeric particulate composites of epoxyresin and metal particles. Compos. Part A Appl. Sci. Manuf. **33**, 375–384 (2002)

39. Thermal Conductivity, hyperphysics.phy-astr.gsu.edu/hbase/thermo/thercond.html. Accessed 28 Sept 2014

40. F.H. Riddle, Ceramic spark-plug insulator. J. Am. Ceram. Soc. **32**(11), 333–346 (1949)